Optical antenna enhanced graphene photodetector

Chitraleema Chakraborty,[1] Ryan Beams,[2] Kenneth M. Goodfellow,[2] G. W. Wicks,[1,2] Lukas Novotny,[3] and A. Nick Vamivakas[1,2,4,a)]
[1]*Materials Science, University of Rochester, Rochester, New York 14627, USA*
[2]*Institute of Optics, University of Rochester, Rochester, New York 14627, USA*
[3]*Photonics Laboratory, ETH Zürich, 8093 Zürich, Switzerland*
[4]*Center for Coherence and Quantum Optics, University of Rochester, Rochester, New York 14627, USA*

(Received 6 October 2014; accepted 4 December 2014; published online 19 December 2014)

We report on the integration of an individual, metal-based, plasmonic nano-antenna on a graphene photodetector. The device exhibits an electromagnetic resonance at a wavelength of 580 nm with well-defined polarization sensitivity. With no applied bias voltage, this antenna-coupled graphene photodetector features a responsivity of ~17 nA/μW, which is four orders of magnitude higher than previously studied single antenna enhanced detectors. Finally, we measure a signal-to-noise ratio of ~200 in a 1-Hz bandwidth, with an average photocurrent value of 1.2 nA. © *2014 AIP Publishing LLC*.
[http://dx.doi.org/10.1063/1.4904800]

Graphene, a single layer of carbon atoms, has become increasingly popular owing to its unique electrical, mechanical, and optical properties.[1–4] Its broadband absorption and ultrafast transport make it an excellent candidate for optoelectronic devices. However, its low absorption, lack of intrinsic bandgap, and low quantum yield inhibit its performance as a photodetector.[5] It is well known that plasmonic based metallic nano-antennas can improve the light harvesting properties of weak light absorbers,[6] so such devices are a natural candidate to improve graphene's optical response.

When a metal nanoparticle (NP) interacts with light, the incident electric field can drive the conduction electrons to collective oscillations known as localized surface plasmon resonance (LSPR). This resonance alters the incident radiation pattern drastically and leads to effects such as subwavelength localization of electromagnetic energy, formation of high intensity hot spots, or anisotropic light scattering angular spectra.[7,8] These effects have already been utilized for modifying the radiative and non-radiative properties of emitters like NP coupled molecules, atoms, or quantum dots.[9,10] Further, metal nanoparticles have been extensively integrated with two-dimensional, atomically thin photodetectors in forms like colloidal particles[11,12] and plasmonic-antenna arrays.[13–16]

Antenna integrated graphene photodetectors have been demonstrated to work in the visible-near infrared (IR),[13] the mid-IR,[17] and the far-IR.[18,19] Most of them show the collective photoresponse from multiple antennas on large area chemical vapor deposition (CVD) graphene photodetectors. In contrast to the previous work, we report on photocurrent enhancement from a lithographically fabricated single nano-antenna with dimensions smaller than ~$\lambda/2$ of light on an exfoliated graphene photodetector. The small detection area has application in nanoscale optoelectronic devices. The previous studies of nano-antenna arrays on graphene motivate the investigation of how an individual antenna can enhance graphene's optical response. Different in our device is that the antenna not only localizes and enhances the illuminating electromagnetic field but it also provides the electrical contacts for extracting light-induced current. Plasmon resonances in individual nano-gap electrodes have also been explored using graphene constrictions,[20] but patterning graphene may open up a bandgap[21] which could limit its spectral responsivity. Additionally, by rationally designing and fabricating a well-defined antenna structure, we are able to control the full electromagnetic response of the antenna.

An illustration of an antenna-on-graphene device with an external electrical circuit for photocurrent detection is presented in Fig. 1(a). We exfoliate graphene from bulk graphite crystals by micromechanical cleavage using adhesive tape.[22] The substrate consists of a doped silicon wafer with a 300 nm thermally grown oxide layer that facilitates single-layer graphene identification under an optical microscope.[1,22,23] Figure 1(b) presents the false color scanning electron microscope (SEM) image of a typical graphene device integrated with an individual nano-antenna. The top inset of Fig. 1(b) shows a magnified SEM image of a fabricated antenna. The antenna is connected to the larger source-drain metal contacts via fingers from the antenna. This enables us to directly read out the graphene electrical signal from light that is localized by the antenna. The device was fabricated using electron beam lithography followed by electron beam metallization with Cr (1 nm)/Au (29 nm). The electrodes were wire-bonded and connected to external electronics. The position and relative intensity of the G and 2D peaks in Raman spectra [bottom inset, Fig. 1(b)] confirm that the flake is single-layer graphene. Also, no disorder induced D band was observed in the Raman spectra indicating that the flake was not damaged during the fabrication.[24] Interestingly, we observe an increase in the intensity of the Raman modes in the antenna-laden graphene region [green curve, bottom inset, Fig. 1(b)] with respect to the antenna-free region (black curve) for 532-nm laser illumination.[13] However, this near-field enhancement is not significantly large due to off-plasmon resonance excitation.

Finite difference time domain (FDTD) (Lumerical software) simulations were used to design the nano-antenna. The length (h) and width (w) of the antenna were 80 nm and

a)Electronic mail: nick.vamivakas@rochester.edu

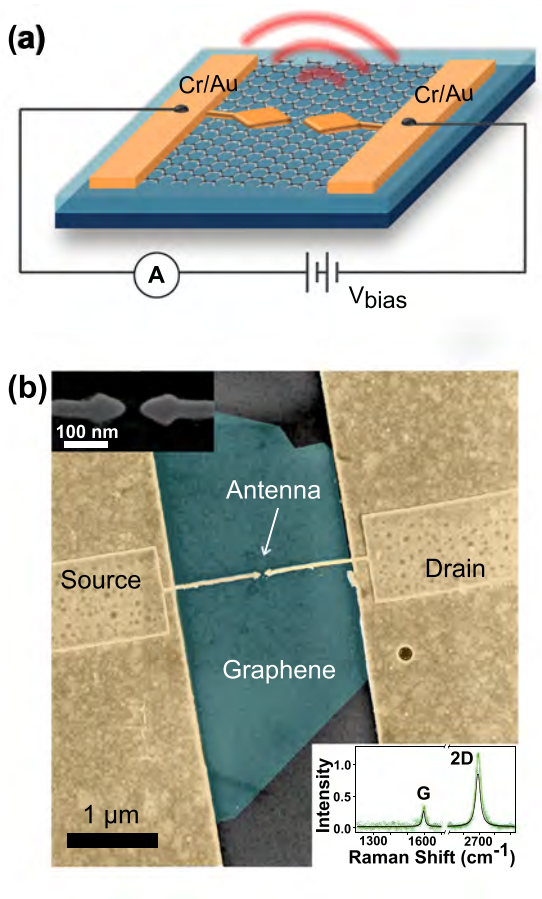

FIG. 1. (a) Illustration showing an antenna-on-graphene device connected to external electronics. (b) False color scanning electron micrograph of a representative antenna-on-graphene device. Inset (top left): zoomed in image of the antenna. Inset (bottom right): Raman spectra of antenna-laden (green) and antenna-free (black) regions of graphene. Solid lines are Lorentzian fits to the data.

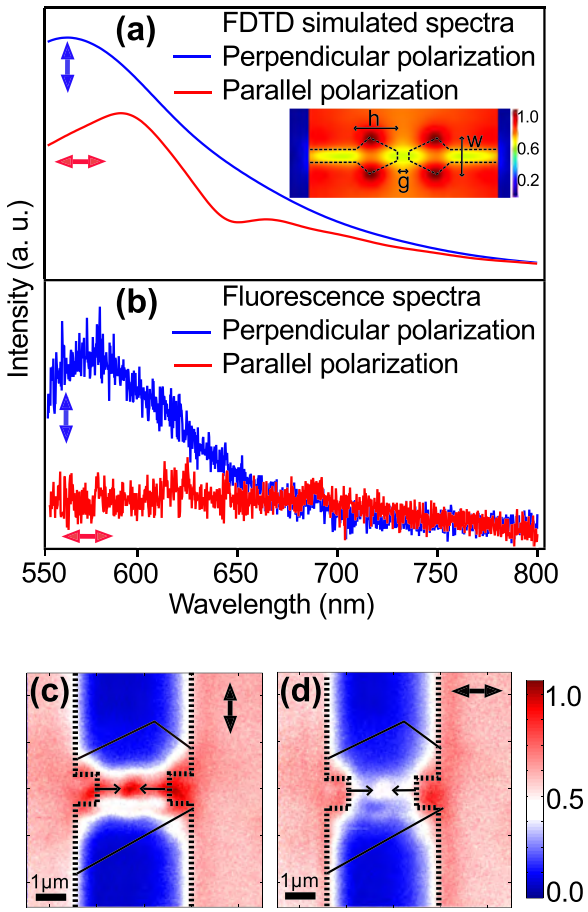

FIG. 2. (a) Normalized FDTD simulated spectra and (b) measured fluorescence spectra showing polarization dependence of gold luminescence of the antenna in perpendicular (blue) and parallel (red) direction of excitation laser. Backgrounds are subtracted. Excitation wavelength, $\lambda = 532$ nm; power = 60 μW. Inset of (a) shows the simulated electromagnetic field distribution of the antenna. (c) and (d) Normalized scanning fluorescence map of the device with laser excitation polarization (c) perpendicular and (d) parallel to the antenna. Dotted lines trace the outline of the contact electrodes and the region within the arrows indicates the enhancement due to the antenna for both (c) and (d). The solid black line outlines the graphene flake between the contact electrodes. Arrows denote the polarization of incident laser.

70 nm, respectively, with 40 nm wide fingers contacting both sides of the antenna (see inset of Fig. 2(a) for the antenna geometry). FDTD simulated scattering spectra of the fabricated antenna show a resonance around 560 nm with a plane wave excitation source linearly polarized. Inset of Fig. 2(a) presents the simulated electromagnetic field distribution of the antenna excited with 532-nm source in perpendicular polarization (along direction of blue arrow). The antenna is outlined in black dashed line as a guide to the eye. The enhancement is maximum around the four corners of the antenna. The resonance is suppressed when the source is polarized parallel to the antenna long-axis. The antenna was designed to exhibit this unconventional polarization response. The main motivation was to mitigate against any possible resonance damping effects that could result from the presence of the metallic fingers connecting the antenna to the electrodes. The broad scattering spectrum exhibited by the antenna is characteristic of a plasmon mediated electromagnetic resonance and is due to damping experienced by charge oscillation of the LSPR when scattering with the nano-structure boundary.[25]

To characterize the optical response of our fabricated antenna, the devices were illuminated with a 532-nm laser, in a home-built inverted confocal microscope, using a microscope objective with a numerical aperture (NA) of 0.75. Figure 2(b) presents the measured fluorescence spectrum. The perpendicular and parallel polarizations correspond to both the polarization orientation of the illuminating laser and the polarization orientation of the fluorescence spectrum collection channel. The fluorescence spectrum confirms that the fabricated nano-antennas exhibit the designed electromagnetic response; they have a plasmon resonance within the visible wavelength range (~580 nm) and in the polarization direction perpendicular to the antenna long axis [Fig. 2(b)]. The difference in resonance peak of our designed structure [inset of Fig. 2(b)] from FDTD simulated structure is due to fabrication imperfections such as surface roughness and size mismatch.[26] In addition to the antenna spectral response, we also acquired scanning fluorescence images of the device. The sample was mounted on a translational stage (Mad City Labs, Inc.) that was raster scanned through the focused laser and photo-counts were recorded with an avalanche photodiode. Evident in the images presented in Figs. 2(c) and 2(d) is that the maximum fluorescence enhancement is obtained when the excitation and collection polarization orientation is

perpendicular to the antenna long axis (the long axis is parallel to the antenna gap).

To investigate the photoresponse of the device, we use a home-built, room temperature, scanning photocurrent (SPC) microscopy setup. The device was illuminated with a laser at excitation wavelength of 635 nm (laser power = 25 μW, NA = 0.8). The sample was raster scanned and a current value was recorded using a Keithley 2400 Sourcemeter. All photocurrent measurements were taken at zero bias to eliminate background current and obtain a gain-free enhancement in photocurrent resulting from the antenna.[27] In Fig. 3(a), a photocurrent map is shown for excitation laser polarized perpendicular to the antenna's long axis. In the SPC map, photocurrent is present in two principal regions: at the source-drain contacts with graphene and in the vicinity of the antenna-on-graphene. Local electric fields are induced at the graphene-electrode junction.[28,29] When light is incident at these junctions, electron-hole pairs are created which generate a photocurrent even at zero bias[30] as a result of structural asymmetry in the device. Figure 3(b) is a second photocurrent map of the same device, exhibiting diminished photocurrent in the antenna region, for laser excitation polarization parallel to the antenna's long axis.

Figure 3(c) [Fig. 3(d)] presents a horizontal line-cut of the current along the antenna in the SPC map from panel (a) [panel (b)] of Fig. 3. The previous line-cuts demonstrate that the current response is antisymmetric at opposing contacts, superimposed with a symmetric plasmon mediated current peak centered around the gap of the antenna. Such antisymmetric photocurrent as a function of position has been previously reported for metal contacts on graphene due to contributions from a thermoelectric effect superimposed with a photovoltaic effect.[28,31] In Figs. 3(e) and 3(f), the antenna response is extracted from the line-cut in panels (c) and (d) by subtracting the symmetric photocurrent response from either end of the antenna response and fit with a symmetric Lorentzian function. Comparing the fluorescence maps [Figs. 2(a) and 2(b)] with the photocurrent maps [Figs. 3(a) and 3(b)], we observe that the maximum polarization sensitivity of photocurrent arises from the same antenna region as obtained from the fluorescence map, which further confirms the plasmonic enhancement from the antenna-on-graphene region.

The polar plot in Fig. 3(g) shows the polarization dependence of the photoresponse from the nano-gap antenna on graphene region, which is consistent with the antenna design and fluorescence spectrum measurements. The polarization contrast $(|I_{max}| - |I_{min}|)/(|I_{max}| + |I_{min}|)$ is 76%. Although the photoresponse is low compared to the previous studies using arrays of antenna on graphene,[13,15] we are able to extract a maximum photoresponse of ~17 nA/μW at zero electrical bias [Fig. 3(h)] from a typical antenna-on-graphene device when illuminated with 66 nW of optical power. This is four orders of magnitude higher than the previous reports on similar single antenna graphene photodetectors.[20] We attribute the increase in photoresponse to light concentration mediated by the antenna and material quality, since our fabrication process does not directly pattern the graphene flake. Furthermore, the quantum efficiency (number of electron-hole pairs detected in the photocurrent per number of incident photons) of this device is calculated to be 3.2% under zero bias and 8.4% for a bias of 0.5 mV [Fig. 3(h)]. We observe that if the quantum efficiency was limited only by graphene absorption, then the maximum value under zero bias would be 2.3%. The increase of quantum efficiency is further evidence of the antenna enhancing the detector's

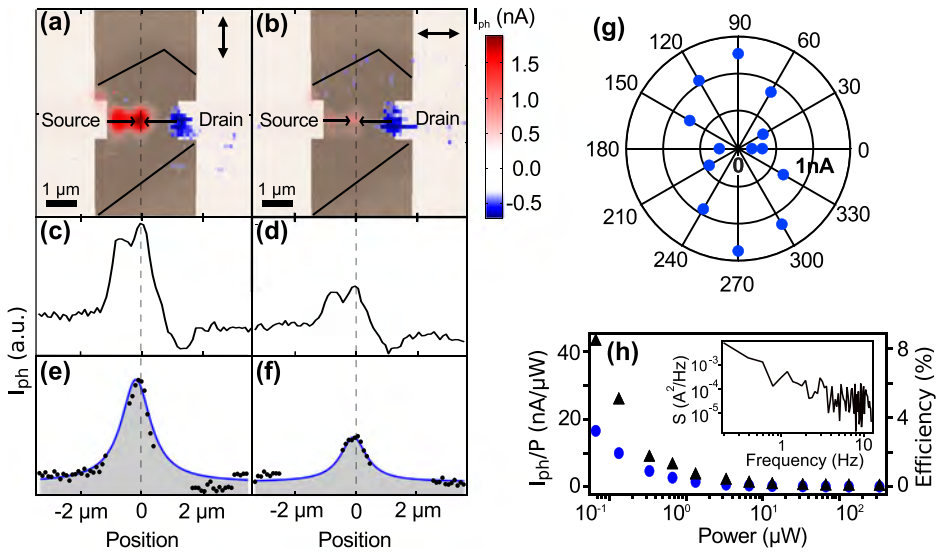

FIG. 3. (a) and (b) Scanning photocurrent image superimposed on a device design with excitation polarization (a) perpendicular and (b) parallel to the antenna's long axis. Color scale denotes photocurrent in nA units. Arrows denote polarization of incident laser. (c) and (d) Horizontal slices of photocurrent through the antenna in panels (a) and (b), respectively, showing a symmetric current response due to antenna superimposed with an antisymmetric response from photodetection at graphene-metal junction. (e) and (f) Contribution in photocurrent from antenna-on-graphene region (area indicated within black arrows in photocurrent map) which is extracted from panels (c) and (d) by subtracting the antisymmetric current from either side of symmetric antenna response. (g) Polar graph showing polarization anisotropy of photocurrent of a typical device. The radius in the polar graph has a photocurrent magnitude of 1.5 nA. Current is maximum for vertical polarization of laser (90°) and minimum for horizontal polarization (0°). (h) Photoresponse (I_{ph}/P) and external quantum efficiency (efficiency) as a function of power showing sub-linear dependence of response for both zero bias (blue circles) and at a bias of 0.5 mV (black triangles). Inset shows the noise power density of the dark current from the detector measured at zero bias.

responsivity. Finally, we determine that our antenna enhanced detector exhibits a signal-to-noise ratio of ~200 in a 1 Hz bandwidth with an average photocurrent value of 1.23 nA measured from a time trace of photocurrent in 40-ms bins (not shown). We also find a noise-equivalent power (NEP) of our detector by taking the noise power spectrum of the background current trace [Inset of Fig. 3(h)] from which we obtain $S(f = 1\,\text{Hz}) = 3.1 \times 10^{-4}\ \text{nA}^2/\text{Hz}$. This determines that the detector NEP to be $1.1 \times 10^{-9}\ \text{W}/\sqrt{\text{Hz}}$ at zero bias.

In conclusion, we have integrated a single optical antenna on a single layer of graphene. The antenna concentrates the illuminating electromagnetic field and also serves as the electrical contacts used for extracting the generated photocurrent. Our approach to enhance the light harvesting ability of a graphene photodetector resulted in responsivities that were nearly four orders of magnitude larger than the previous single antenna devices. It is expected that similar approaches based on optical antennas will also be useful in tailoring the optical response of atomically thin semiconductors.

The authors acknowledge support from the Institute of Optics, the U.S. Department of Energy (Grant No. DE-FG02-05ER46207), the National Science Foundation IGERT program (DGE-0966089), the National Science Foundation (DMR-1309734), the Army Research Office (W911NF1110378), and the Swiss National Science Foundation (200021-149433). The sample used in this work was, in part, fabricated at the Cornell NanoScale Facility, a member of the National Nanotechnology Infrastructure Network, which is supported by the National Science Foundation (Grant No. ECCS-0335765).

[1]K. S. Novoselov, A. K. Geim, S. V. Morozov, D. Jiang, Y. Zhang, S. V. Dubonos, I. V. Grigorieva, and A. A. Firsov, Science **306**, 666 (2004).
[2]R. R. Nair, P. Blake, A. N. Grigorenko, K. S. Novoselov, T. J. Booth, T. Stauber, N. M. R. Peres, and A. K. Geim, Science **320**, 1308 (2008).
[3]C. Lee, X. Wei, J. W. Kysar, and J. Hone, Science **321**, 385 (2008).
[4]K. I. Bolotin, K. Sikes, Z. Jiang, M. Klima, G. Fudenberg, J. Hone, P. Kim, and H. Stormer, Solid State Commun. **146**, 351 (2008).
[5]F. Bonaccorso, Z. Sun, T. Hasan, and A. C. Ferrari, Nat. Photonics **4**, 611 (2010).
[6]J. B. Khurgin and G. Sun, J. Opt. Soc. Am. B **26**, B83 (2009).
[7]V. M. Shalaev, C. Douketis, J. T. Stuckless, and M. Moskovits, Phys. Rev. B **53**, 11388 (1996).
[8]L. Novotny and B. Hecht, *Principles of Nano-Optics* (Cambridge University Press, 2012).
[9]A. G. Curto, G. Volpe, T. H. Taminiau, M. P. Kreuzer, R. Quidant, and N. F. van Hulst, Science **329**, 930 (2010).
[10]O. L. Muskens, V. Giannini, J. A. Sánchez-Gil, and J. Gómez Rivas, Nano Lett. **7**, 2871 (2007).
[11]Y. Shi, J.-K. Huang, L. Jin, Y.-T. Hsu, S. F. Yu, L.-J. Li, and H. Y. Yang, Sci. Rep. **3**, 1839 (2013).
[12]J. Niu, Y. Jun Shin, Y. Lee, J.-H. Ahn, and H. Yang, Appl. Phys. Lett. **100**, 061116 (2012).
[13]Z. Fang, Z. Liu, Y. Wang, P. M. Ajayan, P. Nordlander, and N. J. Halas, Nano Lett. **12**, 3808 (2012).
[14]Y. Yao, M. A. Kats, P. Genevet, N. Yu, Y. Song, J. Kong, and F. Capasso, Nano Lett. **13**, 1257 (2013).
[15]T. J. Echtermeyer, L. Britnell, P. K. Jasnos, A. Lombardo, R. V. Gorbachev, A. N. Grigorenko, A. K. Geim, A. C. Ferrari, and K. S. Novoselov, Nat. Commun. **2**, 458 (2011).
[16]N. K. Emani, T.-F. Chung, X. Ni, A. V. Kildishev, Y. P. Chen, and A. Boltasseva, Nano Lett. **12**, 5202 (2012).
[17]Y. Yao, R. Shankar, P. Rauter, Y. Song, J. Kong, M. Loncar, and F. Capasso, Nano Lett. **14**, 3749 (2014).
[18]L. Vicarelli, M. S. Vitiello, D. Coquillat, A. Lombardo, A. C. Ferrari, W. Knap, M. Polini, V. Pellegrini, and A. Tredicucci, Nat. Mater. **11**, 865 (2012).
[19]M. Mittendorff, S. Winnerl, J. Kamann, J. Eroms, D. Weiss, H. Schneider, and M. Helm, Appl. Phys. Lett. **103**, 021113 (2013).
[20]S.-F. Shi, X. Xu, D. C. Ralph, and P. L. McEuen, Nano Lett. **11**, 1814 (2011).
[21]M. Dvorak, W. Oswald, and Z. Wu, Sci. Rep. **3**, 2289 (2013).
[22]K. S. Novoselov, D. Jiang, F. Schedin, T. J. Booth, V. V. Khotkevich, S. V. Morozov, and A. K. Geim, Proc. Natl. Acad. Sci. U. S. A. **102**, 10451 (2005).
[23]P. Blake, E. W. Hill, A. H. Castro Neto, K. S. Novoselov, D. Jiang, R. Yang, T. J. Booth, and A. K. Geim, Appl. Phys. Lett. **91**, 063124 (2007).
[24]R. Vidano and D. B. Fischbach, J. Am. Ceram. Soc. **61**, 13 (1978).
[25]L. Genzel, T. P. Martin, and U. Kreibig, Z. Phys. B: Condens. Matter **21**, 339 (1975).
[26]Z. Liu, A. Boltasseva, R. H. Pedersen, R. Bakker, A. V. Kildishev, V. P. Drachev, and V. M. Shalaev, Metamaterials **2**, 45 (2008).
[27]A. L. Falk, F. H. L. Koppens, C. L. Yu, K. Kang, N. de Leon Snapp, A. V. Akimov, M.-H. Jo, M. D. Lukin, and H. Park, Nat. Phys. **5**, 475 (2009).
[28]J. Park, Y. H. Ahn, and C. Ruiz-Vargas, Nano Lett. **9**, 1742 (2009).
[29]E. J. H. Lee, K. Balasubramanian, R. T. Weitz, M. Burghard, and K. Kern, Nat. Nanotechnol. **3**, 486 (2008).
[30]F. Xia, T. Mueller, Y.-m. Lin, A. Valdes-Garcia, and P. Avouris, Nat. Nanotechnol. **4**, 839 (2009).
[31]X. Xu, N. M. Gabor, J. S. Alden, A. M. van der Zande, and P. L. McEuen, Nano Lett. **10**, 562 (2010).